Breast Cancer Res Treat (2016) 157:489–501
DOI 10.1007/s10549-016-3844-6

PRECLINICAL STUDY

Therapeutic inhibition of breast cancer bone metastasis progression and lung colonization: breaking the vicious cycle by targeting α5β1 integrin

Hongren Yao[1] · Donna M. Veine[1] · Donna L. Livant[1]

Received: 24 March 2016 / Accepted: 24 May 2016 / Published online: 2 June 2016

Abstract At diagnosis, 10 % of breast cancer patients already have locally advanced or metastatic disease; moreover, metastasis eventually develops in at least 40 % of early breast cancer patients. Osteolytic bone colonization occurs in 80–85 % of metastatic breast cancer patients and is thought to be an early step in metastatic progression. Thus, breast cancer displays a strong preference for metastasis to bone, and most metastatic breast cancer patients will experience its complications. Our prior research has shown that the α5β1 integrin fibronectin receptor mediates both metastatic and angiogenic invasion. We invented a targeted peptide inhibitor of activated α5β1, Ac-PHSCN-NH_2 (PHSCN), as a validated lead compound to impede both metastatic invasion and neovascularization. Systemic PHSCN monotherapy prevented disease progression for up to 14 months in Phase I clinical trial. Here, we report that the next-generation construct, Ac-PhScN-NH_2 (PhScN), which contains D-isomers of histidine (h) and cysteine (c), is greater than 100,000-fold more potent than PHSCN at blocking basement membrane invasion. Moreover, PhScN is also up to 10,000-fold more potent than PHSCN at inhibiting lung extravasation and colonization in athymic mice for both MDA-MB-231 metastatic and SUM149PT inflammatory breast cancer cells. Furthermore, we show that systemic treatment with 50 mg/kg PhScN monotherapy reduces established intratibial MDA-MB-231 bone colony progression by 80 %. Thus, PhScN is a highly potent, well-tolerated inhibitor of both lung colonization and bone colony progression.

Keywords Breast cancer · Invasion · Bone metastasis · Extravasation · Lung metastasis · Integrin fibronectin receptor · Systemic therapy

Abbreviations

SF	Serum free
FBS	Fetal bovine serum
Bio	Biotin
IC50	Concentration for 50 % inhibition
pFn	Plasma fibronectin
DRI	Dose reduction index
DiI	1,1′-Dilinoleyl-3,3,3′3′-tetramethylindocarbocyanine perchlorate
MAP	Multiantigenic peptide
MAb	Monoclonal antibody
SEM	Standard error of mean
Me	Methyl
OAc	Acetyl
μg	Microgram
ng	Nanogram
pg	Picogram
mw	Molecular weight
K_d	Dissociation constant

Background

Metastatic disease develops in 40 % of early breast cancer patients [1] and rapidly metastasizes to bone in 85 % [2, 3]. Bone metastases are osteolytic [2], releasing factors from

✉ Donna L. Livant
dlivant@umich.edu

Hongren Yao
harryao@umich.edu

Donna M. Veine
dveine@umich.edu

[1] Department of Radiation Oncology and Comprehensive Cancer Center, University of Michigan, 1500 East Medical Center Drive, Ann Arbor, MI 48109-5637, USA

the matrix stimulating tumor growth and bone resorption: the "vicious cycle" [2]. Because inflammatory breast cancer (IBC) patients have lymph node involvement and distant metastases at diagnosis, IBC is similar to metastatic breast cancer [1].

Interaction of activated α5β1 integrin fibronectin receptors of metastatic or inflammatory breast cancer cells with the plasma fibronectin (pFn) PHSRN sequence induces constitutive invasion [4]. Moreover, α5β1 regulates invasion [5], angiogenesis [6], extravasation, and colonization by breast and other adenocarcinomas [7–13]. Radiation stimulates invasion by inducing surface upregulation of activated α5β1 integrin [14].

We devised a potent, targeted α5β1 integrin inhibitor, Ac-PHSCN-NH_2 (PHSCN), as a validated lead compound to prevent metastatic [5] and angiogenic invasion [6]. In Phase I clinical trial, systemic PHSCN monotherapy prevented disease progression for up to 14 months [15]. Here, we report that Ac-PhScN-NH_2—containing D-isomers of histidine (h) and cysteine (c)—is over 100,000-fold more potent than PHSCN at blocking basement membrane invasion by MDA-MB-231 and SUM149PT breast cancer cells. We also report that PhScN is 100- to 10,000-fold more potent at inhibiting lung extravasation, and 1000- to 10,000-fold more potent at reducing lung colonization in nude mice. Finally, we report that systemic 50 mg/kg PhScN monotherapy reduces established MDA-MB-231 intratibial colony progression by almost 80 %. Thus, PhScN is a highly potent, well-tolerated inhibitor of bone colony progression.

Materials and methods

Cell lines and cell culture

SUM149PT (Asterand USA, Detroit, MI), MDA-MB-231, and human microvascular endothelial cells (American Type Culture Collection, Manassas, VA) were cultured as recommended, and microscopic morphologies were routinely checked.

Peptide synthesis

N-terminal-acetylated, C-terminal-amidated PhScN, PHSCN, hSPNc, and HSPNC peptides, PhScNGGK-MAP poly-lysine dendrimer, and cysteine or biotinylated (-Bio) derivatives were synthesized and purified to 95 % by Peptide 2.0 (Chantilly, VA), Peptisyntha, Inc. (Torrance, CA) or the University of Michigan Peptide Synthesis Core.

In vitro invasion assays

In vitro invasion assays employing naturally serum-free (SF) basement membranes (SU-ECM) were performed and data analyzed as in [4–9, 14, 16, 17]. Peptides were pre-bound to serum-starved, suspended cells prior to placement on SU-ECM. Mean invasion percentages were analyzed using Prism software (GraphPad Software, San Diego, CA) as a function of log (inhibitor) versus normalized data, variable slope.

Determination of dissociation, K_d, and inhibition constants, K_i, for cell surface binding

PHSCN and PhScN dissociation constants were determined by centrifugation binding assays [18], using biotinylated, N-acetylated, C-amidated Ac-PHSCNGGK-Bio and Ac-PhScNGGK-Bio [9, 12]. Maximal α5β1 activation was promoted by manganese. Binding experiments were performed as pairs to ensure consistency. 150,000 cells, suspended in binding buffer (10 mM HEPES, pH 7.4, 150 mM NaCl, 0.1 % bovine calf serum, and 2 mM $MnCl_2$) were incubated with varying concentrations of biotinylated peptides for 2 h at 4 °C. Washed cell pellets were incubated at 4 °C for 30 min with Streptavidin-peroxidase (Sigma) and *o*-phenylenediamine substrate, stabilized by the addition of HCl. Absorbances were recorded at 490 nM.

Competition assays were performed with a constant concentration of biotinylated peptide and varying amounts of unlabeled competitor. Equilibrium time was 3 h [9]. Binding data were analyzed, and curves were fit using nonlinear regression approaches [9, 19].

Fluorescent DiI labeling of MDA-MB-231 and SUM149PT cells

Washed, confluent cells were suspended and orange fluorescently labeled in SF medium with lipophilic carbocyanine vital dye DiI, 1,1′-dilinoleyl-3,3,3′3′-tetramethylindocarbocyanine perchlorate (Invitrogen) [7–9]. Labeled cells were pelleted, resuspended in 6 ml of medium, and cultured 72 h prior to use.

Mice

Female Foxn1^{nu} athymic nude mice (Harlan) were housed according to the Association for the Assessment and Accreditation for Laboratory Animal Care guidelines. Studies were performed with approved institutional animal use protocols.

Lung extravasation and colonization by MDA-MB-231 or SUM149PT cells

Extravasation-inhibitory potencies of single systemic pretreatments of Ac-PhScN-NH_2, Ac-PHSCN-NH2, or Ac-PhScNGGK-MAP were evaluated using DiI-labeled, peptide- or dendrimer-prebound cells [7–9]. Treated cells were prebound with 1, 10, or 100 ng/ml Ac-PhScN-NH_2; 10, 100, or 1000 ng/ml Ac-PHSCN-NH_2; 1000 ng/ml Ac-HSPNC-NH_2; or 1000 ng/ml Ac-hSPNc-NH_2, for 10 min at 37 °C. Groups of 10 nude mice received one systemic pretreatment with the appropriate peptide concentration by tail vein injection. Immediately thereafter, 10,000 cells, prebound with the appropriate peptide or with HBSS only were injected into tail veins in 0.1 ml HBSS. Mice received no other systemic treatments were euthanized 24 h later, and their lungs were removed. Frozen-tissue samples were prepared, and lung-extravasated cells were quantitated at 400-fold magnification by Zeiss Scanning Laser Confocal microscopy (LSM510). 25 10-μm sections, taken at intervals of 100 μm, were analyzed from one lung in each mouse. Data are presented as mean ± SEM. Mice evaluated for lung colonization were maintained without further treatment for 6 weeks prior to euthanization.

Western blot analysis of activated caspase-3 in SUM149PT cells

Adherent SUM149PT cells were serum-starved overnight, then incubated in serum-containing medium with 0, 10, 50, 100, 200, or 300 μg of Ac-PhScN-NH_2, or 500 μg per 10^6 cells of Ac-hSPNc-NH_2 for 1 h, prior to washing thrice with PBS. Anti-cleaved Caspase 3 MAb (Cell Signaling #9661) primary antibody and horseradish peroxidase HRP-linked anti-rabbit IgG (Cell Signaling, #7074) were used in Western blot analysis of cleaved Caspase-3, as instructed.

Intratibial injection of DiI-labeled MDA-MB-231 cells

Treatment groups of 10 mice were each injected in right tibial crest cortex with 10,000 DiI-labeled MDA-MB-231 cells, not pretreated with peptide [20]. Intratibial colonies progressed untreated for 2 weeks prior to initiation of thrice-weekly PhScN or PHSCN therapies, at 0.0, 5.0, and 50.0 mg/kg. Sterile peptide solutions were prepared in 50 mM HEPES, pH 7.4, and tail vein injected in 100 μl. Mice were euthanized 24 days later, after 10 systemic treatments. Tibia were fixed in 4.0 % paraformaldehyde at 4 °C for 3 days, rinsed in 1.0 % PBS for 2 days, and then stored in 20.0 % sucrose until transfer to a sucrose series in mounting medium, followed by embedding and staining with DAPI, conjugated with green fluorescence-labeled actin [7–9]. Twenty 10-micron sections, separated by 200 microns, were analyzed from each tibia.

Data analysis

Dose response data were analyzed as in [9] by Chou–Talalay Combination index (CI) [21], based on the multiple drug effect equation, where $y = \log(f_a/f_u)$, with respect to $x = \log(\text{dose})$, defines the dose effect relationship without reaction rate constants. f_a is the fraction of cells affected (invasion-inhibited), and f_u is the fraction of cells unaffected (invaded). The x intercept represents the IC50 value. CI and DRI values were determined for Ac-PhScN-NH_2, relative to Ac-PHSCN-NH_2.

Results

Increased invasion-inhibitory potency of Ac-PhScN-NH_2, and Ac-PhScNGGK-MAP

SF SU-ECM basement membranes [9] were utilized to evaluate invasion-inhibitory potencies of S-acetylated or S-methylated PHSCN derivatives [Ac-PHSC(S-OAc)N-NH_2 and Ac-PHSC(S-Me)N-NH_2], the D-His, D-Cys-containing PhScN peptide (Ac-PhScN-NH_2), and the D-His, D-Cys-containing PhScNGGK poly-lysine multi-antigenic peptide dendrimer (Ac-PhScNGGK-MAP) on α5β1-mediated, serum-induced, or SF PHSRN-induced invasion. Figure 1a shows Hill-Slope plots evaluating effects of varying concentrations of Ac-PHSC(S-OAc)N-NH_2, Ac-PHSC(S-Me)N-NH_2, and Ac-PhScN-NH_2 on FCS-induced invasion, compared to Ac-PHSCN-NH_2 (Fig. 1a). To demonstrate that PhScN targets α5β1 integrin-mediated invasion, the α5β1-specific Fn cell-binding domain ligand [22], Ac-PHSRN-NH_2 (PHSRN), was used to induce SF invasion by MDA-MB-231 (Fig. 1b). The alternating L- and D-stereoisomer sequence of Ac-PhScN-NH_2 produced an endoproteinase-resistant peptide with a 100,000-fold increased invasion-inhibitory potency, for serum-induced and SF PHSRN-induced invasion, similar to that achieved by covalent S-modification of the PHSCN cysteine residue. Similar Hill-Slope plots were obtained for SUM149PT (Table 1).

Table 1 summarizes half maximal invasion-inhibitory concentration (IC_{50}) and dose reduction index (DRI) values for PHSCN and S-methylated [C(Me)N] or S-acetylated [C(OAc)N] derivatives for MDA-MB-231 and SUM149PT. IC_{50} and DRI values based on pg/ml or molar (M) concentrations are presented for Ac-PhScN-NH_2 (PhScN) and Ac-PhScNGGK-MAP dendrimer (cN-MAP) for serum- or SF Ac-PHSRN-NH_2 (PHSRN)-induced invasion. Since PhScN is a highly potent inhibitor of SF

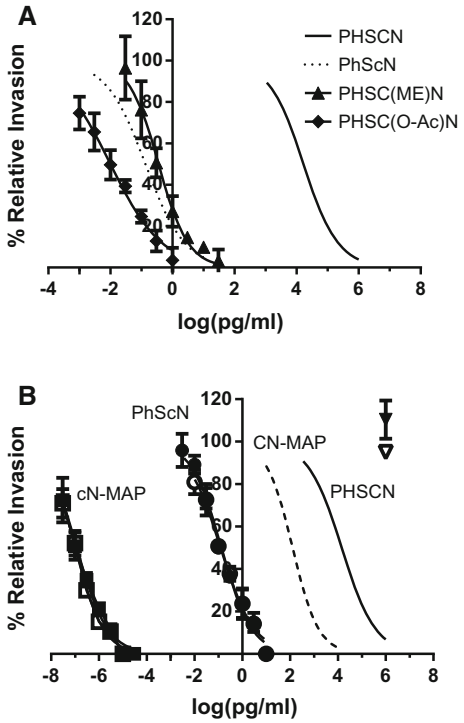

Fig. 1 Hill-slope plots of increased invasion-inhibitory potency of Ac-PhScN-NH_2 peptide, Ac-PhScNGGK-MAP dendrimer, and the cysteine-modified, methylated (Me), or acetylated (OAc) peptides, Ac-PHSC(Me)N-NH_2, and Ac-PHSC(OAc)N-NH_2 for MDA-MB-231 cells. **a** Effects on FBS-induced invasion by cysteine-modified Ac-PHSC(Me)N-NH_2 or Ac-PHSC(OAc)N-NH_2, and D-His, D-Cys containing Ac-PhScN-NH_2 peptides. *Symbols* are denoted in the figure. *X* axis, log peptide concentration in pg per ml; *Y* axis, mean relative percentages of invaded cells (±SD). IC_{50} and DRI values are summarized in Table 1. **b** Increased potencies of PhScN peptide and PhScN dendrimer for both serum-induced and serum-free (SF), Ac-PHSRN-NH_2 (1 μg/ml)-induced, α5β1-mediated invasion. *Circles* denote Ac-PhScN-NH_2; *squares* denote Ac-PhScNGGK-MAP dendrimer; and *triangles* denote Ac-hSPNc-NH_2. *Closed symbols* denote FBS-induced and *open symbols* denote Ac-PHSRN-NH_2 (1 μg/ml) induced, SF invasion. *X* axis, log peptide concentration in pg/ml; *Y* axis, mean relative percentage of invaded cells (±SD). The *solid* and *dashed lines* represent published values for Ac-PHSCN-NH_2 and Ac-PHSCNGGK-MAP, respectively [7]

PHSRN-induced invasion by MDA-MB-231 and SUM149PT, PhScN targets α5β1-mediated invasion in both cell lines.

PHSCN was suggested to inhibit invasion via disulfide bonding with α5β1 integrin [10]. However, increased-inhibitory potencies of the S-acetylated or S-methylated PHSCN derivatives for MDA MB231 and SUM149PT cells, and for prostate cancer [9], suggest that the productive mechanism is noncovalent.

PhScNGGK-MAP (7500 Da), containing 8 subunits of PhScN demonstrated a 10^7-fold increased invasion-inhibitory potency over monomeric PhScN (596 Da), significantly greater than the 1000-fold increase seen when comparing PHSCNGGK-MAP and PHSCN [7, 8] (Fig. 1b; Table 1).

Dissociation constants (K_d) and competition binding assays for cell surface binding using biotinylated PhScN or PHSCN

D-amino acid substitutions change the orientation of the side chains on the PhScN peptide backbone, which could affect target binding and explain the 100,000-fold increase in PhScN invasion-inhibitory potency. A binding assay, developed to determine the dissociation constant (K_d) of biotin-labeled PHSCN peptide to suspended cells [10], was utilized to compare the K_d's of biotinylated PhScN and PHSCN peptides. The invasion-inhibitory potencies of biotinylated PHSCN and PhScN were confirmed on SU-ECM. IC_{50}'s of Ac-PhScNGGK-Bio and Ac-PHSCNGGK-Bio were similar to those of Ac-PhScN-NH_2 and Ac-PHSCN-NH_2, respectively, for suspended MDA-MB-231 (Fig. 2a; Table 2) and SUM149PT (Table 2).

As shown in Fig. 2b and summarized in Table 2, K_d's for Ac-PHSCNGGK-Bio binding to suspended SUM149PT and MDA-MB-231 cells were 0.028 and 0.032 μM, respectively. K_d values for Ac-PhScNGGK-Bio were 0.029 and 0.053 μM for suspended SUM 149PT and MDA-MB-

Table 1 Inhibition of α5β1-mediated invasion of basement membranes by SUM149PT and MDA-Mb-231 cells: IC50 and DRI values for PhScN and PHSCN derivatives

	Mw	SUM149 PT		MDA-MB-231		DRI	
		IC_{50}		IC_{50}			
		FBS pg/ml	PHSRN pg/ml	FBS pg/ml	PHSRN pg/ml	pg/ml	M
PHSCN	598	8980	67,120	16,800	14,500	1	1
CN-MAP	7500	125	152	128	90	10^2	10^3
C(Me)N	614	0.27	–	0.36	–	10^4	10^4
C(OAc)N	640	0.01	–	0.01	–	10^6	10^6
PhScN	598	0.076	0.081	0.135	0.124	10^5	10^5
cN-MAP	7500	4.4×10^{-8}	7.6×10^{-8}	1.3×10^{-7}	1.1×10^{-7}	10^{11}–10^{12}	10^{12}–10^{13}

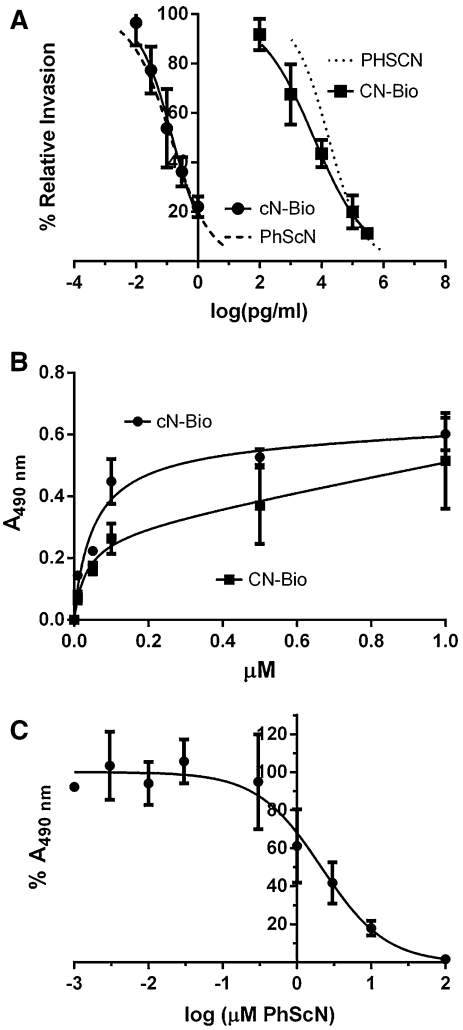

Fig. 2 **a** Hill-slope plots of invasion inhibition by biotinylated derivatives of PHSCN and PhScN for MDA-MB-231 cells induced by FBS. Specific agents (CN-Bio, Ac-PHSCNGGK-Bio; cN-Bio, Ac-PhScNGGK-Bio) are listed on the *right*. *X* axis, log peptide concentration in pg per ml; *Y* axis, mean relative percentages of invaded cells (±SD). IC_{50} and DRI values are summarized in Table 2. **b** K_d binding assays for Ac-PHSCNGGK-Bio (CN-Bio) and Ac-PhScNGGK-Bio (cN-Bio) peptides with suspended MDA MB231 cells. Plots were fit using a total binding equation to account for nonspecific binding [19]. **c** Competition binding was determined by incubating suspended MDA-MB-231 cells with a constant concentration of 0.1 μM Ac-PHSCNGGK-Bio (labeled) and varying amounts of unlabeled Ac-PhScN-NH_2. Plot was fitted using the Motulsky and Neubig competitive inhibition equation [19]

231, respectively. Since PhScN and PHSCN K_d values were similar, the improved invasion-inhibitory potency of PhScN (Table 1) is due to elimination of the nonproductive covalent side reaction by orienting the D-His and D-Cys side chains to the opposite side of the peptide ligand, rather than to tighter binding, as for prostate cancer [9]. Thus, noncovalent interaction is key to invasion-inhibitory potency.

Competition assays were also performed to confirm that PHSCN and PhScN interact with the same binding site on breast cancer cells, like prostate cancer [9]. Results of assays, in which suspended MDA-MB-231 cells were incubated with a constant concentration (0.1 μM) of biotinylated Ac-PHSCNGGK-Bio and varying concentrations of Ac-PhScN-NH_2, are presented in Fig. 2c. They show that dissociation of Ac-PHSCNGGK-Bio with increasing concentrations of unlabeled Ac-PhScN-NH_2 occurs over 2 orders of magnitude, demonstrating that PhScN and PHSCN compete for the same binding site on MDA-MB-231 [19], as for SUM149PT, *not shown*.

Increased lung extravasation inhibition by PhScN and PhScNGGK-MAP

Lung extravasation-inhibitory efficacies of PhScN and PhScNGGK-MAP were compared with PHSCN in nude mice. As shown in Fig. 3a, the mean number of extravasated MDA-MB-231 and SUM149PT cells per section was decreased by 100- to 1000-fold by Ac-PhScN-NH_2, and by at least 100,000-fold by Ac-PhScNGGK-MAP, relative to Ac-PHSCN-NH_2. The median-effect plot of Fig. 3b shows that increasing concentrations of PhScN or PHSCN, or PhScNGGK-MAP dendrimer, log-linearly decrease SUM149PT and MDA-MB-231 extravasation, with similar relative potencies. Pretreatment with 1 μg per ml Ac-hSPNc-NH_2 scrambled sequence control, followed by a single systemic treatment at the equivalent dose, had no inhibitory effect on extravasation, *not shown*. As summarized in Table 3, Ac-PhScN-NH_2 is 100- to 1000-fold more potent than Ac-PHSCN-NH_2 at inhibiting SUM149PT and MDA-MB-231 lung extravasation, and Ac-PhScNGGK-MAP is 100,000- to 1000,000-fold more potent. These in vivo values correlate with those seen in SU-ECM invasion assays (Table 1), and are similar to

Table 2 Invasion inhibition: IC_{50} and K_d 's for biotinylated PhScN and PHSCN derivatives

	Mw	SUM149 PT		MDA-MB-231	
		IC_{50} (pg/ml)	K_d (μM)	IC_{50} (pg/ml)	K_d (μM)
Ac-PHSCN-NH_2	598	8980	NA	16,800	NA
Ac-PhScN-NH_2	598	0.076	NA	0.124	NA
Ac-PHSCNGGK-Bio	1100	8637	0.028 ± 0.02	5622	0.032 ± 0.03
Ac-PhScNGGK-Bio	1100	0.051	0.029 ± 0.02	0.15	0.053 ± 0.03

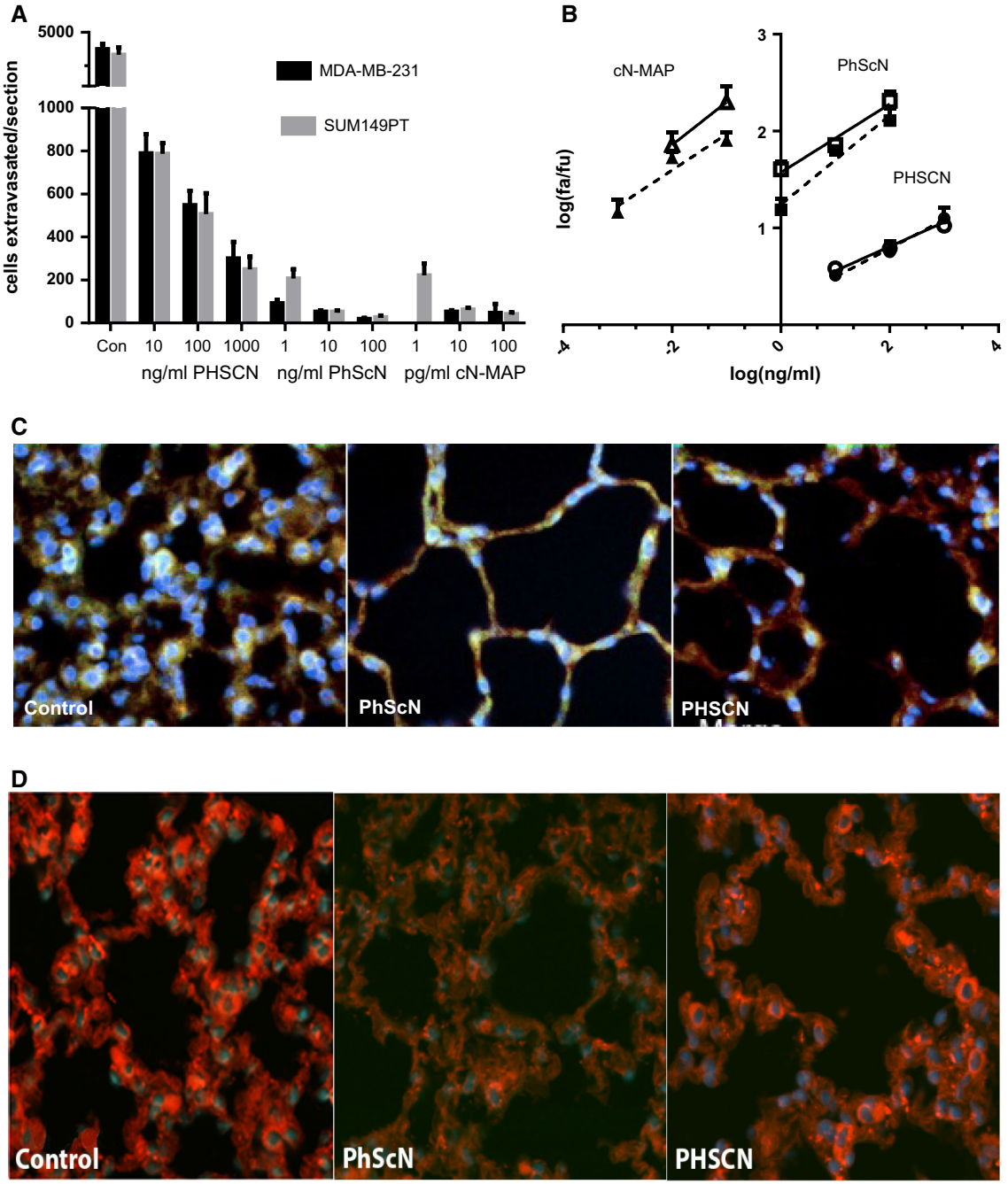

Fig. 3 Increased extravasation inhibition by Ac-PhScN-NH_2 or Ac-PhScNGGK-MAP prebinding, relative to Ac-PHSCN-NH_2 peptide. **a** *Y* axes, average cells extravasated/section; *X* axes, Con, control; 10, 100, 1000 ng/ml PHSCN; 1, 10, 100 ng/ml PhScN; 1, 10, 100 pg/ml PhScNGGK-MAP. **b** Median-effect plot for extravasation into lung after prebinding with PHSCN (*circles*), PhScN (*squares*) or PhScN-MAP (*triangles*); *open symbols* MDA-MB231 cells; *closed symbols* SUM 149 PT cells. *X* axes, log peptide concentration in ng/ml; *Y* axes, mean log fraction affected/fraction unaffected (f_a/f_u) ± SEM. IC_{50} and DRI values are summarized in Table 3. **c** Typical examples of sectioned lung tissue for MDA-MB231 extravasation analyzed by confocal microscopy after pretreatment with 100 ng/ml Ac-PhScN-NH_2 or 100 ng/ml Ac-PHSCN-NH_2, compared to untreated control. **d** Typical examples of sectioned lung tissue for SUM149PT extravasation analyzed by confocal microscopy after pretreatment with 100 ng/ml Ac-PhScN-NH_2 or 1000 ng/ml Ac-PHSCN-NH_2, compared to untreated control. Images represent the merged composite of DiI-labeled cells shown in *orange*; blue stained nuclei from DAPI Mounting Medium; green tissue from actin staining. (Color figure online)

those observed for metastatic prostate cancer [9]. Figure 3c, d shows typical examples of sectioned lung tissue for MDA-MB-231 and SUM149PT extravasation, obtained by confocal microscopic analysis after pretreatment with 100 ng/ml Ac-PhScN-NH_2 or 100 ng/ml Ac-PHSCN-NH_2, versus untreated or scrambled sequence controls.

Table 3 Extravasation Inhibition, IC50's and DRI values for PhScN, PHSCN, and the PhScNGGK-dendrimer, cN-MAP

	Mw	SUM149PT IC_{50} pg/ml	MDA-MB-231 IC_{50} pg/ml	DRI	
				pg/ml	M
PHSCN	598	214	61	1	1
PhScN	598	2.0	0.036	10^2–10^3	10^2–10^3
cN-MAP	7500	0.0005	0.0006	10^5	10^6

Increased potency of PhScN peptide as an inhibitor of lung colonization

Since extravasated cells may not establish a metastasis [23], effects of PhScN or PHSCN pretreatment on lung colonization were determined by allowing extravasated cells to grow 6 weeks without further treatment. Figure 4a shows the comparison of the effects of prebinding various concentrations of PhScN or PHSCN to suspended, DiI-labeled SUM149PT or MDA-MB-231 on lung colonization after tail vein injection. Dose response curves in Fig. 4b are median-effect plots, and the IC_{50} and DRI values are summarized in Table 4. Both PhScN and PHSCN pretreatment log-linearly decreased MDA-MB-231 and SUM149PT lung colonization. PhScN was 3850-fold more potent than PHSCN for reducing SUM149PT lung colony formation, and 32,143-fold more potent for MDA-MB-231. Furthermore, since all of the 120 control (untreated, Ac-HSPNC-NH_2- or Ac-hSPNc-NH_2-treated) mice, injected intravenously with suspended SUM149PT or MDA-MB-231 cells, had to be euthanized to prevent suffering due to respiratory distress, while none of the PhScN-treated mice did, systemic PhScN therapy may also be a more potent inhibitor of respiratory distress due to lung metastasis progression. Figure 4c shows the examples of DiI-labeled MDA-MB-231 colonies in fluorescent actin- and DAPI-stained lung tissue after no treatment, and after prebinding of the injected cells to 100 ng/ml of either PHSCN or PhScN. SUM149PT lung colonies had a similar appearance, *data not shown*.

Since stress activates α5β1 [24], and apoptosis induction could increase PhScN potency, we assessed apoptosis in vitro by examining effects of a 1-h treatment with a range of Ac-PhScN-NH_2 concentrations. Figure 4d presents a typical Western blot indicating that PhScN rapidly induces dose-dependent upregulation of activated Caspase-3 in adherent SUM149PT. However, the concentrations are 1000- to 100,000-fold higher than those required for lung colonization inhibition. Lack of effect of an elevated concentration of a scrambled sequence control, 500 μg Ac-hSPNc-NH_2 per 10^6 SUM149PT cells, is also shown. Lack of activated Caspase-3 upregulation in SUM149PT cells treated with hSPNc demonstrates that although elevated PhScN concentrations are required for activated Caspase-3 upregulation, the effect is sequence specific.

PhScN exhibits a similar increase in lung colonization-inhibitory potency, relative to PHSCN, for MDA-MB-231 and SUM149PT (1000- to 10,000-fold). However, the corresponding IC_{50} values are 10- to 100-fold higher for SUM149PT (Table 4)—perhaps due to differences between metastatic and inflammatory cancer cell lines—the DRI values suggest that PhScN is 1000- to 10,000-fold more potent at preventing lung colonization than PHSCN for both MDA-MB-231 and SUM149PT.

Inhibition of MDA-MB-231 bone metastasis progression by systemic PhScN

Breast cancer bone metastasis occurs earlier than lung colonization [3]. Interaction with surrounding bone marrow and matrix is described by the "vicious cycle" model [2], in which parathyroid hormone-related protein (PTHrP) expressed by breast cancer cells after bone colonization [25], stimulates progression and enhances osteoclastic bone resorption [24, 26–28]. Metastatic breast cancer cell signals induce osteoblasts to express osteoclast stimulatory factors [29], stimulating multinucleated osteoclasts to resorb mineralized bone matrix [30–32] and release sequestered growth factors that interact with their receptors to promote metastatic growth by stimulating angiogenesis [33–36]. Activated α5β1 receptors of microvascular endothelial cells interact with the pFn PHSRN sequence to induce angiogenic invasion [6]. Matrix metalloproteinase-1 (MMP1), induced by α5β1 FnR binding to PHSRN, mediates both angiogenic and metastatic invasion by breast, prostate, and pancreatic cancer cells [4–6, 14]. MMP-1 activates the protease activated receptor-1 (PAR-1) gene in both breast cancer [37] and endothelial cells [38], thereby promoting breast cancer invasion and angiogenesis. PTHrP stimulates osteoblasts to induce progenitor differentiation into active osteoclasts which mediate bone resorption, releasing epidermal growth factor (EGF)-like growth factors to further stimulate bone metastasis progression [39]. Overexpression of receptor tyrosine-protein kinase erbB-2 (HER2) induces α5β1-mediated, mammary epithelial cell invasion [40], due to surface downregulation of the invasion-inhibitory α4β1 integrin [41]. Furthermore, MDA-MB-231 colonies in the bones of athymic mice can induce angiogenesis in osteolytic metastases [36]. Identification of α5β1 as the primary integrin fibronectin receptor on human bone marrow stroma [42] suggests that PhScN could be effective in reducing bone metastases. These interactions and the potential inhibitory effects of PhScN therapy on α5β1-mediated breast cancer (BC) and angiogenic invasion are diagrammed in Scheme 1.

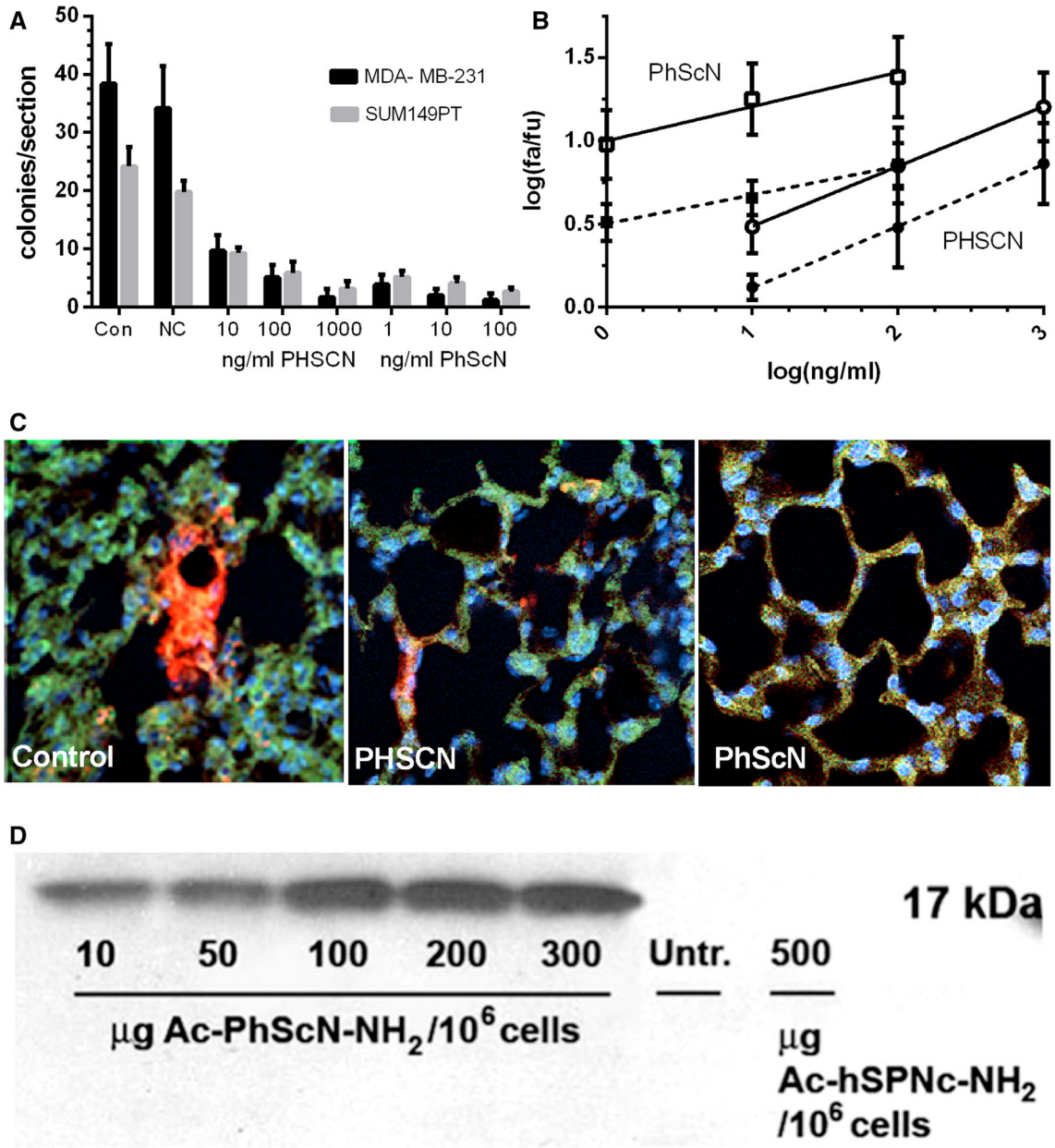

Fig. 4 Increased inhibition of lung colonization by Ac-PhScN-NH_2 prebinding, relative to Ac-PHSCN-NH_2. **a** *Y* axes, average colonies/section; *X* axes, Con, control; NC, 100 ng/ml HSPNC or hSPNc; 10, 100, 1000 ng/ml PHSCN; 1, 10, 100 ng/ml PhScN. **b** Median-effect plot for lung colony formation after prebinding to PHSCN (*circles*) or PhScN (*squares*). *Closed symbols*, *dotted lines* SUM149PT cells; *open symbols*, *solid lines* MDA-MB-231 cells. *X* axes, log peptide concentration in ng/ml. *Y* axes, mean log fraction affected/fraction unaffected (f_a/f_u) ± SEM. IC_{50} and DRI values are summarized in Table 4. **c** Typical examples of sectioned lung tissue for MDA-MB-231 colonization analyzed by confocal microscopy after pretreatment with 100 ng/ml Ac-PhScN-NH_2 or 100 ng/ml Ac-PHSCN-NH_2 compared to untreated control. Images represent the merged composite of DiI-labeled cells shown in *orange*; blue stained nuclei from DAPI Mounting Medium; green tissue from actin staining. **d** Example of a typical Western blot showing dose-dependent upregulation of activated Caspase-3 in adherent SUM149PT cells by a 1-h treatment with a range of Ac-PhScN-NH_2 concentrations (10, 50, 100, 200, or 300 µg/10^6 cells). Micrograms of Ac-PhScN-NH_2 per million SUM149PT cells are indicated. Lack of effects of an elevated concentration of a scrambled sequence control, 500 µg Ac-hSPNc-NH_2 per 10^6 SUM149PT cells, is also shown. (Color figure online)

We evaluated microvascular endothelial cell (hmvec) invasion in vitro as described [6]; PHSCN and PhScN were confirmed to block invasion. The IC_{50} values were similar to those determined for MDA-MB-231 and SUM149PT. PhScN demonstrated a 6.3×10^4-fold increase in potency over PHSCN (PhScN IC_{50}, 1.3×10^{-13} M; PHSCN IC_{50}, 8.4×10^{-9} M).

Table 4 Effects of PHSCN or PhScN pretreatment on lung colonization

	SUM149PT IC50 pg/ml	MDA-MB-231 IC50 pg/ml	DRI	
			pg/ml	M
PHSCN	4890	450	1	1
PhScN	1.27	0.014	10^3–10^4	10^3–10^4

To compare the effects of PHSCN and PhScN on established bone metastases, DiI-labeled, untreated MDA-MB-231 cells were injected intratibially and allowed to grow into intra-osteal colonies for 2 weeks before thrice-weekly systemic treatments of 5 or 50 mg/kg of PhScN or PHSCN were initiated. Systemic treatments were continued for 24 days. Each mouse received a total of 10 systemic treatments. As shown in Fig. 5a, 50 mg/kg systemic PhScN monotherapy reduced bone colony progression by 77 %, compared to 57 % for 50 mg/kg PHSCN. Median-effect analyses, Fig. 5b, indicate a dosage IC_{50} of 0.4 mg/kg for PhScN and 10 mg/kg for PHSCN. The DRI values indicate that PhScN is 25-fold more potent than PHSCN as a systemic inhibitor of bone metastasis progression. As seen in confocal microscopy examples, Fig. 5c, few cells remained in the bone marrow of 50 mg/kg PhScN-treated mice; significantly more were present in marrows of mice treated with 50 mg/kg PHSCN. Bone colonies appeared to be either extravascular, or closely associated with the vasculature.

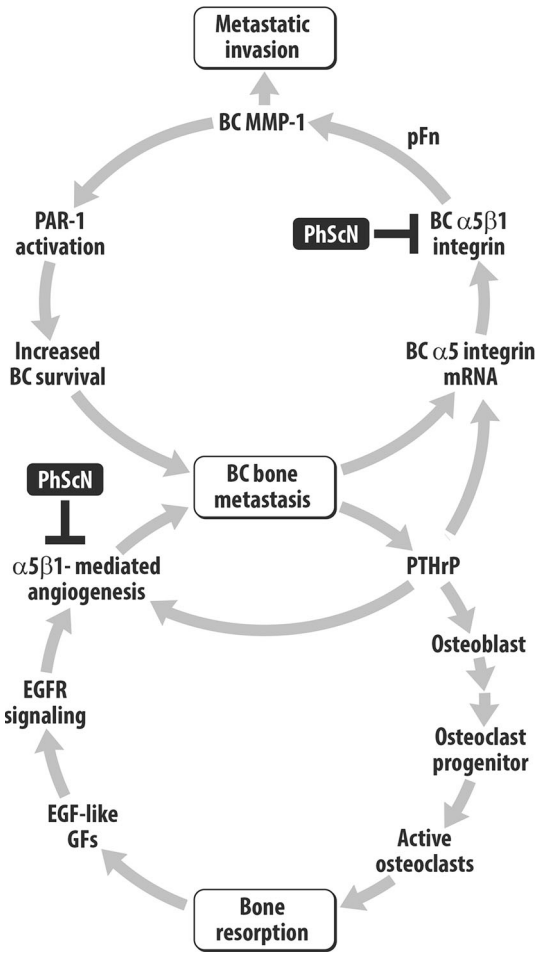

Scheme 1 Vicious cycle model of breast cancer bone metastasis. *BC* breast cancer, *MMP-1* matrix metalloproteinase-1 interstitial collagenase, *PTHrP* parathyroid hormone-related protein, *EGF-like GFs* epidermal growth factor-like growth factors, *EGFR* epidermal growth factor receptor

Colocalization of Ac-PhScNGGK-Bio with DiI in extravasated breast cancer cells

Since nodal metastases occur in at least 20 % of patients undergoing completion axillary lymph node dissection (ALND) following a positive sentinel lymph node biopsy (SLNB), the use of SLNB alone for axilla staging underestimates nodal disease [43]. Hence, a more efficient means of detecting metastatic disease would be beneficial. Ac-PhScNGGK-Bio might be an efficient detection agent for extravasated breast cancer cells in sectioned biopsies. Thus, we assessed Ac-PhScNGGK-Bio/DiI colocalization in tail vein-injected, lung-extravasated SUM149PT cells. As shown in Fig. 6a, a range of Ac-PhScNGGK-Bio concentrations (1.0–50.0 μg per ml) labeled 89–90 % of extravasated cells 24 h after injection, suggesting that labeled PhScN is efficient agent for detecting extravasated breast cancer cells. Figure 6b shows representative images of extravasated DiI-labeled SUM149PT, with and without Ac-PhScNGGK-Bio.

Discussion

Since recurrent or metastatic disease develops in 40 % of early breast cancer patients [1], with bone metastasis in most [2], there is an urgent need for effective therapy to prevent metastatic and angiogenic invasion. As summarized in Scheme 1, inhibition of activated α5β1 receptors on metastatic breast cancer and associated microvascular endothelial cells may form the basis of an effective targeted therapy to inhibit the vicious cycle of bone metastasis progression. Because overexpression of PTHrP in MDA-MB-231 cells induces a 10- to 25-fold upregulation of α5 integrin expression and increased α5β1 integrin [44], and because α5β1 mediates metastatic invasion, systemic dissemination [4, 5, 14, 16, 45], and microvascular endothelial cell invasion [6], α5β1 is a key therapeutic target [4–9, 14, 17].

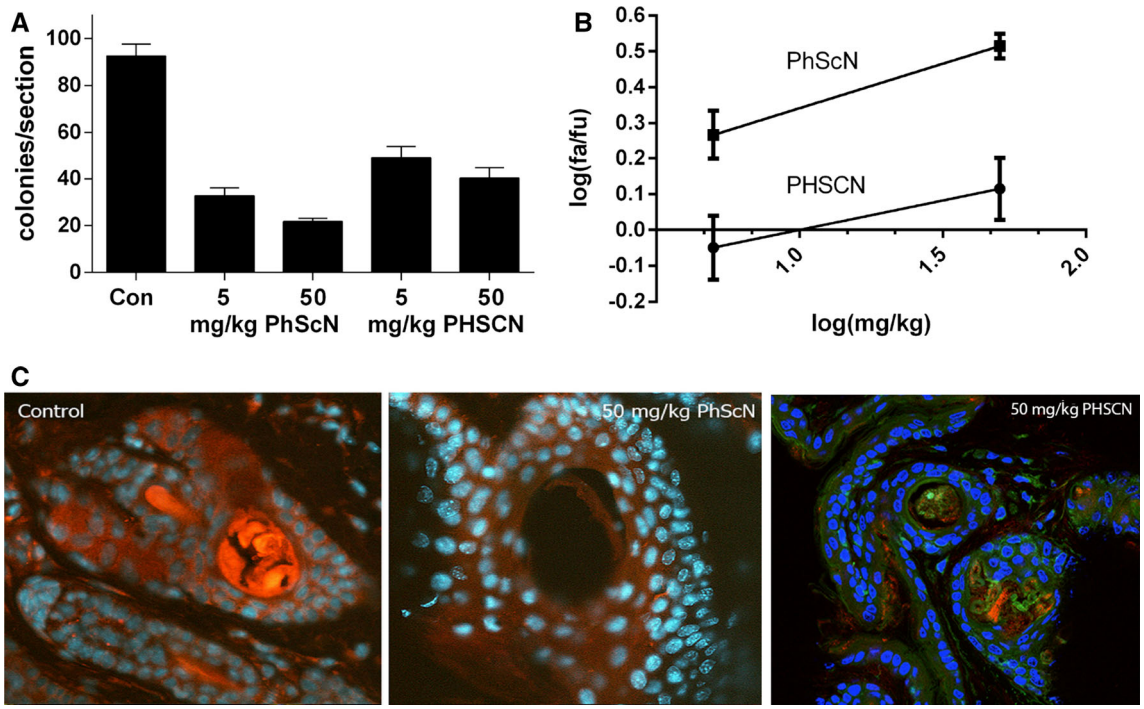

Fig. 5 Increased potency of PhScN as a systemic therapy to prevent breast cancer bone colony progression in athymic mice. **a** Anti-metastatic potencies of systemic PhScN (Ac-PhScN-NH_2) versus PHSCN (Ac-PHSCN-NH_2) for reducing MDA-MB-231 bone marrow progression in athymic mice. *Y* axes, average colonies per section; *X* axes, Con, untreated control; 5 and 50 mg/kg PhScN; 5 and 50 mg/kg PHSCN. **b** Median-effect plot for effects of PhScN versus PHSCN on bone marrow progression, *X* axis, log peptide dosage level (mg/kg); *Y* axis, mean log fraction affected/fraction unaffected (f_a/f_u) ± SEM. **c** Examples of bone marrow from untreated mice, and from mice treated with a total of 10 thrice-weekly tail vein injections of 50 mg/kg PhScN or 50 mg/kg PHSCN. Images represent the merged composite of DiI-labeled cells shown in *orange*; stained nuclei from DAPI Mounting Medium in *blue*; tissue from actin staining in *green*. Thus, DiI-labeled cells appear *orange* (Control) or *green* with *orange* inclusions (50 mg/kg PHSCN). No DiI-labeled cells appear in the image of sectioned bone from mice receiving 50 mg/kg PhScN. (Color figure online)

Scheme 1 suggests that by targeting α5β1, PhScN may inhibit both angiogenesis and breast cancer bone invasion, as well as reducing bone resorption through its inhibitory effects on PTHrP- and growth factor-mediated signaling. We report that D-His, D-Cys-containing PhScN peptide is 10^5-fold more potent than PHSCN as an inhibitor of α5β1-mediated, basement membrane invasion, 100- to 1000-fold more potent as an inhibitor of lung extravasation, and 3800- to 32,000-fold more potent at reducing lung colonization, when the effects of a single exposure to each peptide were compared. Since all untreated, HSPNC- or hSPNc-treated mice had to be euthanized to prevent suffering due to respiratory distress from the effects of SUM149PT or MDA-MB-231 overgrowth of their lungs, systemic PhScN therapy might also be able to reduce suffering due to lung metastasis progression in breast cancer patients.

Results were also presented showing that the multivalent presentation of PhScN sequence increases its relative potency on a molar basis by an additional 10^8-fold as an in vitro invasion inhibitor, or by an additional 1000- to 10,000-fold as a lung extravasation inhibitor. Consistent with the key role of α5β1-mediated invasion in metastatic progression [4–6], we also report that systemic PhScN monotherapy was well-tolerated and reduced bone colony progression. Our results also suggested that labeled PhScN is an efficient agent for detecting extravasated, potentially metastatic breast cancer cells, due to surface-activated α5β1 integrin expression.

Advanced breast cancer patients are currently treated with Denosumab anti-receptor activator of nuclear factor kappa-B (RANK) ligand MAb or zoledronic acid to manage the bone metastasis symptoms and delay skeletal related events (SRE). However, neither treatment delays disease progression or increases overall survival [46–48]. In contrast, PhScN monotherapy demonstrated a nearly 80 % reduction of bone colony progression on established intra-osteal colonies. Thus, by targeting α5β1 receptors PhScN may offer the opportunity to slow disease progression and break the vicious cycle.

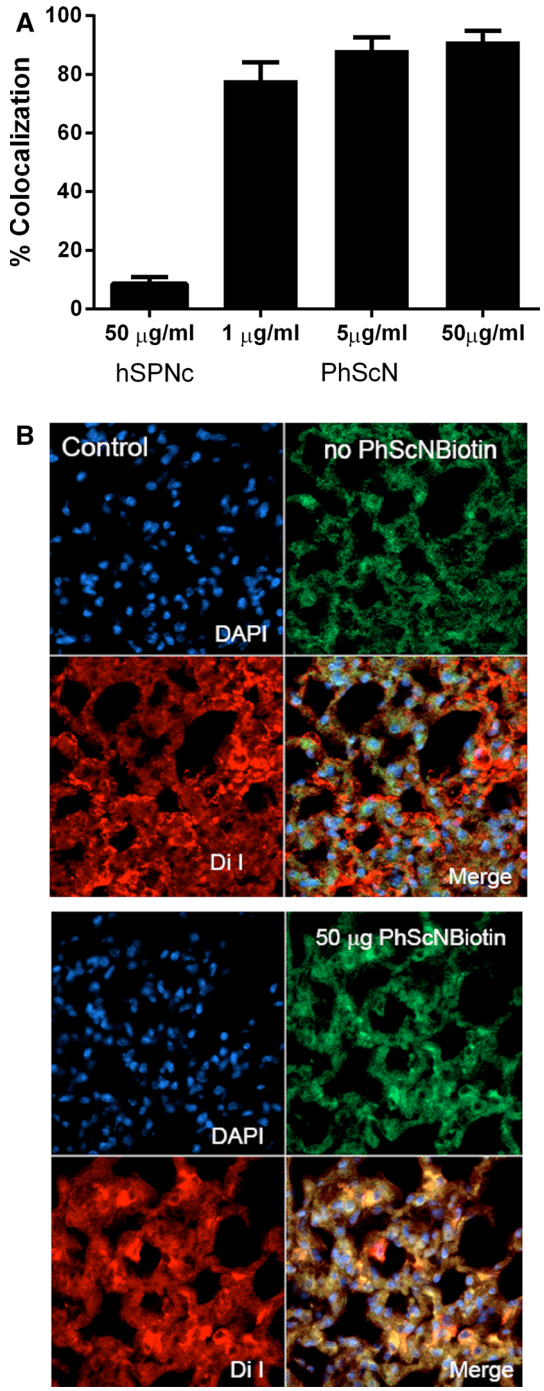

Fig. 6 Colocalization of Ac-PhScNGGK-Bio with DiI in lung-extravasated SUM149PT cells. **a** Percentage of DiI-labeled cells in lung tissue binding to different concentrations of Ac-PhScNGGK-Bio: 1, 5, or 50 μg per ml. *X* axis, binding agents: hSPNc, Ac-hSPNc-NH_2 (a scrambled sequence control peptide); PhScN, Ac-PhScNGGK-Bio. *Y* axis, mean percentage of biotinylated, DiI-labeled SUM149PT cells (±SEM). **b** Examples of fluorescently stained lung tissue: control, no PhScNGGK-Bio; 50 μg PhScNGGK-Bio, 50 μg per ml Ac-PhScNGGK-Bio. DiI-labeled cells shown in *orange*; stained nuclei from DAPI Mounting Medium in *blue*; tissue from actin staining in *green*. (Color figure online)

Acknowledgments The authors wish to thank Steve Kronenberg in the Department of Radiation Oncology, University of Michigan for drawing the bone metastasis model depicted in Scheme 1. We also wish to thank the University of Michigan Office of Technology Transfer for their work on patent 8,940,701: *Compounds for, and methods of treating cancer and inhibiting invasion and metastases.* The in vitro studies and lung metastasis research described here were supported by a Department of Defense Idea Expansion Award F028579. The bone metastasis research described here was supported by a grant from the Michigan Economic Development Corporation, through the University of Michigan Medical School's Strategic Research Initiative, U-M MTRAC for Life Sciences.

Authors' contributions Hongren Yao performed all of the tissue preparations and confocal microscopic studies necessary for the analysis of the effects of PhScN on lung extravasation and lung colonization. He also performed all of the intratibial injections and tissue preparations, as well as all of the confocal microscopic analysis of bone marrow progression. Donna Veine performed all of the K_d determinations, competition binding assays, in vitro invasion assay preparations, data analysis, figure preparation and assisted in manuscript writing. Donna Livant performed all of the in vitro invasion assay data collections, as well as planning and directing the project, and writing the manuscript.

Compliance with ethical standards

Conflict of interest The author, Donna Livant, received salary from the University of Michigan, which owns the patent on her invention, patent 8,940,701: *Compounds for, and methods of treating cancer and inhibiting invasion and metastases.* The authors, Hongren Yao and Donna Veine declare that they have no competing interests.

References

1. Dickson RB, Lippman ME (2001) Cancer of the breast. In: DeVita VT, Hellman S, Rosenberg SA (eds) Cancer: principles & practice of oncology, 6th edn. Lippencott Williams & Wilkins, Philadelphia, pp 1633–1726
2. Mundy GR (2002) Metastasis to bone: causes, consequences and therapeutic opportunities. Nat Rev Cancer 2(8):584–593. doi:10.1038/nrc867
3. Husemann Y, Geigl JB, Schubert F, Musiani P, Meyer M, Burghart E, Forni G, Eils R, Fehm T, Riethmuller G, Klein CA (2008) Systemic spread is an early step in breast cancer. Cancer Cell 13(1):58–68. doi:10.1016/j.ccr.2007.12.003
4. Jia Y, Zeng ZZ, Markwart SM, Rockwood KF, Ignatoski KM, Ethier SP, Livant DL (2004) Integrin fibronectin receptors in matrix metalloproteinase-1-dependent invasion by breast cancer and mammary epithelial cells. Cancer Res 64(23):8674–8681. doi:10.1158/0008-5472.CAN-04-0069
5. Livant DL, Brabec RK, Pienta KJ, Allen DL, Kurachi K, Markwart S (2000) Upadhyaya A anti-invasive, antitumorigenic, and antimetastatic activities of the PHSCN sequence in prostate carcinoma. Cancer Res 60(2):309–320
6. Zeng Z-Z, Yao H, Staszewski ED, Rockwood KF, Markwart SM, Fay KS, Spalding AC, Livant DL (2009) (alpha)5(beta)1 integrin ligand PHSRN induces invasion and (alpha)5 mRNA in endothelial cells to stimulate angiogenesis. Transl Oncol 2:8–20
7. Yao H, Veine D, Fay K, Staszewski E, Zeng Z-Z, Livant D (2011) The PHSCN dendrimer as a more potent inhibitor of human breast cancer cell invasion, extravasation, and lung colony formation. Breast Cancer Res Treat 125:363–375

8. Yao H, Veine DM, Zeng ZZ, Fay KS, Staszewski ED, Livant DL (2010) Increased potency of the PHSCN dendrimer as an inhibitor of human prostate cancer cell invasion, extravasation, and lung colony formation. Clin Exp Metastasis 27(3):173–184. doi:10.1007/s10585-010-9316-1
9. Veine DM, Yao H, Stafford DR, Fay KS, Livant DL (2014) A D-amino acid containing peptide as a potent, noncovalent inhibitor of alpha5beta1 integrin in human prostate cancer invasion and lung colonization. Clin Exp Metastasis 31:379–393. doi:10.1007/s10585-013-9634-1
10. Donate F, Parry GC, Shaked Y, Hensley H, Guan X, Beck I, Tel-Tsur Z, Plunkett ML, Manuia M, Shaw DE, Kerbel RS, Mazar AP (2008) Pharmacology of the novel antiangiogenic peptide ATN-161 (Ac-PHSCN-NH2): observation of a U-shaped dose-response curve in several preclinical models of angiogenesis and tumor growth. Clin Cancer Res 14:2137–2144
11. van Golen KL, Bao L, Brewer GJ, Pienta KJ, Kamradt JM, Livant DL, Merajver SD (2002) Suppression of tumor recurrence and metastasis by a combination of the PHSCN sequence and the antiangiogenic compound tetrathiomolybdate in prostate carcinoma. Neoplasia 4(5):373–379. doi:10.1038/sj.neo.7900258
12. Khalili P, Arakelian A, Chen G, Plunkett ML, Beck I, Parry GC, Donate F, Shaw DE, Mazar AP, Rabbani SA (2006) A non-RGD-based integrin binding peptide (ATN-161) blocks breast cancer growth and metastasis in vivo. Mol Can Ther 5:2271–2280
13. Stoeltzing O, Liu W, Reinmuth N, Fan F, Parry GC, Parikh AA, McCarty MF, Bucana CD, Mazar AP, Ellis LM (2003) Inhibition of integrin alpha5beta1 function with a small peptide (ATN-161) plus continuous 5-FU infusion reduces colorectal liver metastases and improves survival in mice. Int J Cancer 104:496–503
14. Yao H, Zeng Z-Z, Fay KS, Veine DM, Straszewski ED, Morgan MA, Wilder-Romans K, Williams TM, Spalding AC, Ben-Josef E, Livant DL (2011) Role of alpha5beta1 integrin upregulation in radiation-induced invasion by human pancreatic cancer cells. Transl Oncol 4(5):282–292
15. Cianfrocca ME, Kimmel KA, Gallo J, Cardoso T, Brown MM, Hudes G, Lewis N, Weiner L, Lam GN, Brown SC, Shaw DE, Mazar AP, Cohen RB (2006) Phase 1 trial of the antiangiogenic peptide ATN-161 (Ac-PHSCN-NH(2)), a beta integrin antagonist, in patients with solid tumours. Br J Cancer 94(11):1621–1626. doi:10.1038/sj.bjc.6603171
16. Zeng Z-Z, Jia YF, Hahn NJ, Markwart SM, Rockwood KF, Livant DL (2006) Role of focal adhesion kinase and phosphatidylinositol 3′-kinase in integrin fibronectin receptor-mediated, matrix metalloproteinase-1 dependent invasion by metastatic prostate cancer cells. Cancer Res 66(16):8091–8099
17. Livant DL, Brabec RK, Kurachi K, Allen DL, Wu Y, Andrews P, Ethier SP, Markwart S (2000) The PHSRN sequence induces extracellular matrix invasion and accelerates wound healing in obese diabetic mice. J Clin Invest 105(11):1537–1545
18. Hulme EC (1992) Centrifugation binding assays. In: Hulme EC (ed) Receptor–ligand interactions: a practical approach. Oxford University Press, Oxford, pp 235–246
19. Motulsky HJ, Neubig RR. Analyzing binding data. Current protocols in neuroscience/editorial board, Jacqueline N Crawley [et al] 2010; Chapter 7:Unit 7 5. doi:10.1002/0471142301.ns0705s52
20. Hall CL, Dai J, van Golen KL, Keller ET, Long MW (2006) Type I collagen receptor (alpha 2 beta 1) signaling promotes the growth of human prostate cancer cells within the bone. Cancer Res 66(17):8648–8654. doi:10.1158/0008-5472.CAN-06-1544
21. Chou TC, Talalay P (1984) Quantitative analysis of dose–effect relationships: the combined effects of multiple drugs or enzyme inhibitors. Adv Enzyme Regul 22:27–55
22. Aota S, Nomizu M, Yamada KM (1994) The short amino acid sequence Pro-His-Ser-Arg-Asn in human fibronectin enhances cell-adhesive function. J Biol Chem 269(40):24756–24761
23. Gupta GP, Massague J (2006) Cancer metastasis: building a framework. Cell 127(4):679–695. doi:10.1016/j.cell.2006.11.001
24. Jean C, Gravelle P, Fournie JJ, Laurent G (2011) Influence of stress on extracellular matrix and integrin biology. Oncogene 30(24):2697–2706. doi:10.1038/onc.2011.27
25. Suva LJ, Winslow GA, Wettenhall RE, Hammonds RG, Moseley JM, Diefenbach-Jagger H, Rodda CP, Kemp BE, Rodriguez H, Chen EY et al (1987) A parathyroid hormone-related protein implicated in malignant hypercalcemia: cloning and expression. Science 237(4817):893–896
26. Alonso V, de Gortazar AR, Ardura JA, Andrade-Zapata I, Alvarez-Arroyo MV, Esbrit P (2008) Parathyroid hormone-related protein (107–139) increases human osteoblastic cell survival by activation of vascular endothelial growth factor receptor-2. J Cell Physiol 217(3):717–727. doi:10.1002/jcp.21547
27. Esbrit P, Alvarez-Arroyo MV, De Miguel F, Martin O, Martinez ME, Caramelo C (2000) C-terminal parathyroid hormone-related protein increases vascular endothelial growth factor in human osteoblastic cells. J Am Soc Nephrol 11(6):1085–1092
28. Isowa S, Shimo T, Ibaragi S, Kurio N, Okui T, Matsubara K, Hassan NM, Kishimoto K, Sasaki A (2010) PTHrP regulates angiogenesis and bone resorption via VEGF expression. Anticancer Res 30(7):2755–2767
29. Guise TA (1997) Parathyroid hormone-related protein and bone metastases. Cancer 80(8 Suppl):1572–1580
30. Kong YY, Yoshida H, Sarosi I, Tan HL, Timms E, Capparelli C, Morony S, Oliveira-dos-Santos AJ, Van G, Itie A, Khoo W, Wakeham A, Dunstan CR, Lacey DL, Mak TW, Boyle WJ, Penninger JM (1999) OPGL is a key regulator of osteoclastogenesis, lymphocyte development and lymph-node organogenesis. Nature 397(6717):315–323. doi:10.1038/16852
31. Blair HC, Teitelbaum SL, Ghiselli R, Gluck S (1989) Osteoclastic bone resorption by a polarized vacuolar proton pump. Science 245(4920):855–857
32. Delaisse JM, Engsig MT, Everts V, del Carmen Ovejero M, Ferreras M, Lund L, Vu TH, Werb Z, Winding B, Lochter A, Karsdal MA, Troen T, Kirkegaard T, Lenhard T, Heegaard AM, Neff L, Baron R, Foged NT (2000) Proteinases in bone resorption: obvious and less obvious roles. Clin Chim Acta 291(2):223–234
33. Tang X, Zhang Q, Shi S, Yen Y, Li X, Zhang Y, Zhou K, Le AD (2010) Bisphosphonates suppress insulin-like growth factor 1-induced angiogenesis via the HIF-1alpha/VEGF signaling pathways in human breast cancer cells. Int J Cancer 126(1):90–103. doi:10.1002/ijc.24710
34. Peoples GE, Blotnick S, Takahashi K, Freeman MR, Klagsbrun M, Eberlein TJ (1995) T lymphocytes that infiltrate tumors and atherosclerotic plaques produce heparin-binding epidermal growth factor-like growth factor and basic fibroblast growth factor: a potential pathologic role. Proc Natl Acad Sci USA 92(14):6547–6551
35. Petersen M, Pardali E, van der Horst G, Cheung H, van den Hoogen C, van der Pluijm G, Ten Dijke P (2010) Smad2 and Smad3 have opposing roles in breast cancer bone metastasis by differentially affecting tumor angiogenesis. Oncogene 29(9):1351–1361. doi:10.1038/onc.2009.426
36. Winding B, Misander H, Sveigaard C, Therkildsen B, Jakobsen M, Overgaard T, Oursler MJ, Foged NT (2000) Human breast cancer cells induced angiogenesis, recruitment, and activation of osteoclasts in osteolytic metastasis. J Cancer Res Clin Oncol 126(11):631–640
37. Boire A, Covic L, Agarwal A, Jacques S, Sherifi S, Kuliopulos A (2005) PAR1 is a matrix metalloprotease-1 receptor that

promotes invasion and tumorigenesis of breast cancer cells. Cell 120(3):303–313. doi:10.1016/j.cell.2004.12.018
38. Blackburn JS, Brinckerhoff CE (2008) Matrix metalloproteinase-1 and thrombin differentially activate gene expression in endothelial cells via PAR-1 and promote angiogenesis. Am J Pathol 173(6):1736–1746. doi:10.2353/ajpath.2008.080512
39. Foley J, Nickerson N, Riese DJ 2nd, Hollenhorst PC, Lorch G, Foley AM (2012) At the crossroads: EGFR and PTHrP signaling in cancer-mediated diseases of bone. Odontology 100(2):109–129. doi:10.1007/s10266-012-0070-5
40. Ignatoski KM, Maehama T, Markwart SM, Dixon JE, Livant DL, Ethier SP (2000) ERBB-2 overexpression confers PI 3′ kinase-dependent invasion capacity on human mammary epithelial cells. Br J Cancer 82(3):666–674. doi:10.1054/bjoc.1999.0979
41. Woods Ignatoski KM, Grewal NK, Markwart S, Livant DL, Ethier SP (2003) p38MAPK induces cell surface alpha4 integrin downregulation to facilitate erbB-2-mediated invasion. Neoplasia 5(2):128–134
42. Van der Velde-Zimmermann D, Verdaasdonk MA, Rademakers LH, De Weger RA, Van den Tweel JG, Joling P (1997) Fibronectin distribution in human bone marrow stroma: matrix assembly and tumor cell adhesion via alpha5 beta1 integrin. Exp Cell Res 230(1):111–120. doi:10.1006/excr.1996.3405
43. Noguchi M, Morioka E, Ohno Y, Noguchi M, Nakano Y, Kosaka T (2013) The changing role of axillary lymph node dissection for breast cancer. Breast Cancer 20(1):41–46. doi:10.1007/s12282-012-0416-4
44. Anderson JA, Grabowska AM, Watson SA (2007) PTHrP increases transcriptional activity of the integrin subunit alpha5. Br J Cancer 96(9):1394–1403. doi:10.1038/sj.bjc.6603720
45. Korah R, Boots M, Wieder R (2004) Integrin alpha5beta1 promotes survival of growth-arrested breast cancer cells: an in vitro paradigm for breast cancer dormancy in bone marrow. Cancer Res 64(13):4514–4522. doi:10.1158/0008-5472.CAN-03-385364/13/4514
46. Stopeck AT, Lipton A, Body JJ, Steger GG, Tonkin K, de Boer RH, Lichinitser M, Fujiwara Y, Yardley DA, Viniegra M, Fan M, Jiang Q, Dansey R, Jun S, Braun A (2010) Denosumab compared with zoledronic acid for the treatment of bone metastases in patients with advanced breast cancer: a randomized, double-blind study. J Clin Oncol 28(35):5132–5139. doi:10.1200/JCO.2010.29.7101
47. Fizazi K, Carducci M, Smith M, Damiao R, Brown J, Karsh L, Milecki P, Shore N, Rader M, Wang H, Jiang Q, Tadros S, Dansey R, Goessl C (2011) Denosumab versus zoledronic acid for treatment of bone metastases in men with castration-resistant prostate cancer: a randomised, double-blind study. Lancet 377(9768):813–822. doi:10.1016/S0140-6736(10)62344-6
48. Henry DH, Costa L, Goldwasser F, Hirsh V, Hungria V, Prausova J, Scagliotti GV, Sleeboom H, Spencer A, Vadhan-Raj S, von Moos R, Willenbacher W, Woll PJ, Wang J, Jiang Q, Jun S, Dansey R, Yeh H (2011) Randomized, double-blind study of denosumab versus zoledronic acid in the treatment of bone metastases in patients with advanced cancer (excluding breast and prostate cancer) or multiple myeloma. J Clin Oncol 29(9):1125–1132. doi:10.1200/JCO.2010.31.3304